Molecular dynamics simulations of simple monatomic amorphous nanoparticles

Vo Van Hoang[1,*] and T. Odagaki[2]

[1]*Department of Physics, Institute of Technology, National University of HochiMinh City, 268 Ly Thuong Kiet Street, District 10, HochiMinh City, Vietnam*

[2]*Department of Physics, Kyushu University, Fukuoka 812-8581, Japan*

(Received 23 September 2007; revised manuscript received 15 January 2008; published 27 March 2008)

Monatomic amorphous nanoparticles were studied in a spherical model containing different numbers of atoms ranging from 1189 to 9093 by using molecular dynamics method under nonperiodic boundary conditions. We use the double-well interaction pair potential developed by Engel and Trebin, and amorphous nanoparticles were obtained by cooling from the melts. The structural properties of nanoparticles were studied via radial distribution function, mean atomic distances, coordination number, and bond-angle distributions. In addition, we also analyzed local order in nanoparticles by using the technique proposed by Honeycutt and Andersen, and we found the existence of icosahedral order in the system. We found strong size effects on the static properties of nanoparticles. Aging effects on the structure of nanoparticles were also observed and discussed. The radial atomic density profile of nanoparticles was found and discussed. On the other hand, the surface and core structures of nanoparticles were studied in detail. Moreover, we found the size dependence of several quantities such as the glass transition temperature (T_g), the potential energy, and surface energies of nanoparticles. The mean-squared displacement of atoms was discussed.

DOI: 10.1103/PhysRevB.77.125434 PACS number(s): 61.46.−w, 78.55.Qr, 61.43.Bn

I. INTRODUCTION

Nanoscaled systems have been intensively investigated by both experiments and computer simulations in recent years not only due to their enormous technological importance, but also due to scientific interests.[1–16] Nanoparticles often exhibit structures and properties significantly different from the corresponding bulk counterparts. On the other hand, while crystalline nanoparticles have been under intensive studies, it was given less attention to the amorphous nanoparticles, which may be due to their low abundance compared with the crystalline counterparts.[6–11] Therefore, our understanding of their structure and properties is still limited although amorphous nanoparticles have been obtained in practice and they are an important form of nanomaterials in addition to the crystalline ones.[6–11] Moreover, detailed information on an atomistic level of structure and properties of nanoscaled systems can be found just by computer simulation, and one can find only a few works carried out in this direction.[12–17] The physical properties of vitreous and amorphous Si nanoparticles containing 400, 500, and 600 atoms have been studied via molecular dynamics (MD) simulation. However, most attention was paid to the local structure and diffusion constant in the system.[12] The structural properties of amorphous TiO_2 spherical nanoparticles were studied in MD simulation models with different sizes of 2, 3, 4, and 5 nm under nonperiodic boundary conditions.[13] They used the pairwise interatomic potentials proposed by Matsui and Akaogi, and significant size effects were found on the partial radial distribution functions, coordination number distributions, bond-angle distributions, and interatomic distances. The calculated surface energy of amorphous TiO_2 nanoparticles has reasonable value, and it is close to that of the crystalline counterpart. More comprehensive MD simulation was done for the liquid and amorphous SiO_2 nanoparticles, in which the size dependence of the glass transition temperature was found and discussed in addition to the role of structural defects.[15] On the other hand, a good review of the structural properties of free nanoclusters can be found in Ref. 16, in which much attention was paid to the interplay of energetic, thermodynamic, and kinetic factors in the explanation of cluster structures that were actually observed in the experiments. It is essential to note that Lennard-Jones (LJ) clusters, i.e., the simple nanoscaled systems, have been under intensive investigations for the past decades[17–24] and much attention was paid to the melting or freezing or local structural order in the systems. In contrast, less attention was paid to the glass transition and structural properties of simple amorphous nanoscaled systems although it was found recently that the amorphous structure of Lennard-Jones Ar confined in a nanoscale pore is "practically stable" in the sense that no crystallization is observed during 40 ns of annealing.[17] So far, our knowledge of structure and properties of liquid and amorphous nanoparticles is still poor, and it is of interest to carry out the study on simple monatomic liquid and amorphous nanoparticles since we can focus our attention only on the topological order in the structure rather than on both topological and chemical orders. Therefore, it motivates us to carry out a comprehensive study of the size effects on the structural and thermodynamic properties of simple monatomic amorphous nanoparticles by using the double-well interatomic pair potential, similar to that of Dzugutov,[25] which was recently proposed by Engel and Trebin.[26]

II. CALCULATIONS

We performed the simulations in spherical nanoparticles containing different numbers of identical atoms, i.e., it contains 1189, 2469, 3407, 5743, and 9093 atoms, which were denoted model (1), model (2), model (3), model (4), and model (5), respectively. We used nonperiodic boundary conditions with an elastic reflection behavior. The form of the

TABLE I. Parameters of LJG potential with a glass-forming ability and structural quantities of well-relaxed models at $T=0.1$. All models contain 2744 atoms in a cube under periodic boundary conditions. Here, $\bar{r}$ is the mean interatomic distance, $\bar{Z}$ is the mean coordination number, and R_o is a cutoff radius for the determination of coordination number. We use $\sigma_0^2=0.02$ [models (B)–(D) were obtained by using *NPT* ensemble, while the remaining models were obtained by using *NVT* one].

Model	r_0	ε_0	$\bar{r}$	$\bar{Z}$	T_g	R_o
(A)	1.20	1.50	1.160	13.31	0.33	1.45
(B)	1.20	2.50	1.175	13.69	0.53	1.45
(C)	1.20	3.50	1.195	13.66	0.64	1.45
(D)	1.20	4.50	1.200	13.56	0.67	1.45
(E)	1.47	1.50	0.904	11.73	0.46	1.25
(F)	1.47	2.50	0.900	11.96	0.64	1.25
(G)	1.47	3.50	0.880	11.76	0.69	1.20

interatomic potential used in the present work is given below:

$$V(r)=\varepsilon\left\{\left(\frac{\sigma}{r}\right)^{12}-2\left(\frac{\sigma}{r}\right)^{6}+\varepsilon_0\exp\left[-\frac{(r-r_0)^2}{2\sigma_0^2}\right]\right\}. \quad (1)$$

For most values of the parameters, i.e., $\varepsilon_0\in[0.10,5.00]$, $r_0\in[1.11,2.10]$, and $\sigma_0^2=0.02$ (see Ref. 26), $V(r)$ is a double-well potential with the second well at position r_0, depth ε_0, and width σ_0. This potential was called Lennard-Jones–Gauss (LJG) and it was initially proposed for the self-assembly of two-dimensional monatomic complex crystals and quasicrystals. However, in three-dimensional systems, the situation is quite different. We found that stable glassy configurations can be obtained by using the LJG potential with limited values for the parameters r_0 and ε_0, especially when we use relatively small values for r_0 (see Table I). In contrast, crystallization occurs if we use r_0 with larger values and quasicrystals have not been found yet (not shown). In particular, a stable glassy state in both nanoparticles and in the bulk can be obtained if we use the potential with the parameters such as $r_0=1.47$, $\varepsilon_0=1.50$, and $\sigma_0^2=0.02$, and we used such fixed parameters in the present work. It is essential to note that in order to test the stability of an amorphous structure, we have a relaxed amorphous model with $r_0=1.47$, $\varepsilon_0=1.50$, and $\sigma_0^2=0.02$ containing 2744 atoms in a cube under periodic boundary conditions, which is obtained at $T=0.3$ by using *NVT* ensemble simulation for 5×10^6 MD steps (or 6.175 ns if Ar is taken for testing), and its amorphous structure remains unchanged during such relatively long annealing. In contrast, it was found that the bulk argon glass with a pure Lennard-Jones potential is much easier to crystallize, i.e., it transforms into the closest-packed crystal just after the annealing of 0.045–0.300 ns (see Ref. 17). Therefore, one can consider that the glassy state with LJG potential used in the present work is practically stable in the sense that no crystallization is observed during a relatively long time of annealing like that discussed in Ref. 17. Further, the cutoff was applied to the LJG potential at $r=2.5$ similar to what was done in Ref. 26. The initial spherical configuration was cut from a big simple cubic structure model, which was previously built at the density $\rho_0=0.8$. Such initial configuration melted by a further relaxation for 5×10^4 MD steps at a high temperature $T=1.0$ (*NVT* ensemble simulation). Then the system was cooled down from the melt at constant volume corresponding to the system density $\rho_0=0.8$ (i.e., *NVT* quenching). Temperature of the system was linearly decreased in time as $T=T_0-\gamma n$. Here, $\gamma=10^{-5}$ per MD step is the cooling rate, n is the number of MD steps, and $T_0=1.0$ is the initial temperature. We use the Verlet algorithm, and the MD time step is $dt=0.005\tau_0$. We use the following LJ-reduced units in the present work: the length in units of σ, temperature T in units of ε/k_B, and time in units of $\tau_0=\sigma\sqrt{m/\varepsilon}$ [see Eq. (1) and Fig. 1]. Here, k_B is the Boltzmann constant and m is the atomic mass. For Ar, $\sigma=3.84$ Å (i.e., it is the atomic diameter of Ar), $m=6.632\times10^{-26}$ kg, and, by taking the energy unit $\varepsilon=1.0$ eV, we can infer that the time unit $\tau_0=0.247$ ps and the MD time step $dt=0.005\tau_0=1.235$ fs. This means that the cooling rate used in the present work is equal to 0.810×10^{10} K/s. This value of the cooling rate is close to those analytically suggested for freezing of liquid nanodroplets in Ref. 16. However, it is essential to note that we use the one-step cooling of the system from the liquid state to the glassy state. In order to calculate the coordination number and bond-angle distributions in nanoparticles, we adopt the fixed value $R_o=1.25$. Here, R_o denotes a cutoff radius, which is chosen as the position of the minimum after the first peak in the radial distribution function (RDF) for the amorphous state at the temperature of $T=0.1$. The final amorphous configuration at

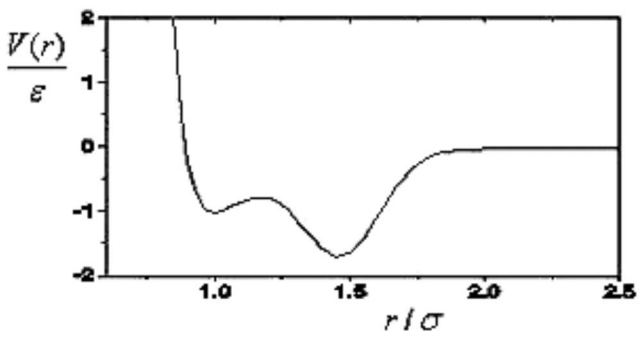

FIG. 1. LJG potential with $r_0=1.47$, $\varepsilon_0=1.50$, and $\sigma_0^2=0.02$.

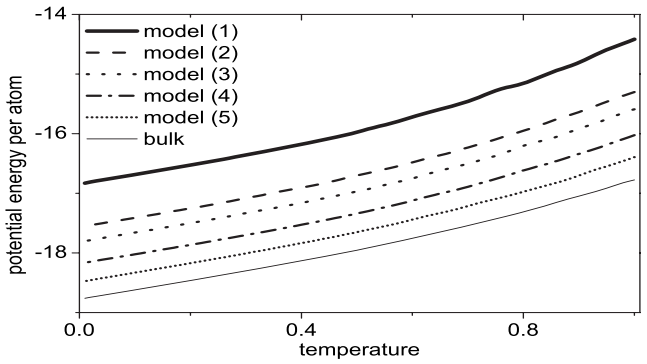

FIG. 2. Temperature dependence of the potential energy of nanoparticles.

$T=0.1$ was relaxed for 5×10^4 MD steps (or 61.75 ps if we take Ar for testing; this time is large enough for equilibrating the MD simulation system) before calculating static quantities. The diameters of nanoparticles in the present work are $d=14$, 18, 20, 24, and 28σ, respectively. It was kept constant during the calculations for each nanoparticle. By taking Ar for testing with $\sigma=3.84$ Å, we found that the sizes (or diameter) of the nanoparticles are equal to 5.376, 6.912, 7.680, 9.216, and 10.752 nm for models (1), (2), (3), (4), and (5), respectively. For comparison, we also show the results for liquid and amorphous models in a cube containing 9261 atoms under periodic boundary conditions, which are considered as the bulk counterparts. In order to improve the statistics, we average the results over two independent runs. It is essential to note that similar double-well interaction potentials were previously proposed in order to clarify the mechanism of the density anomaly of water[27,28] or for the self-assembly of simple lattices.[29]

III. RESULTS AND DISCUSSIONS

A. Glass transition and thermodynamics

The curve for an interatomic LJG potential is presented in Fig. 1, where one can clearly see two wells of the potential. It is essential to note that the general form of pair potentials in metals consists of a strong repulsive core plus a decaying oscillatory Friedel term. Therefore, the LJG potential can be understood like an oscillatory potential cutting off after the second minimum,[26] and in this part of the paper, we focus our attention on the glass transition and the thermodynamics of liquid and amorphous nanoparticles. Figure 2 shows that the potential energy of nanoparticles decreases with decreasing temperature upon cooling from the melt. On the other hand, one can see that E_{pot} (the potential energy per atom) for nanoparticles is significantly higher than that for the bulk due to the surface energy of the former. Thus, we can suggest the following relations:

$$E_{pot}^{nano} - E_{pot}^{bulk} = e_s, \tag{2}$$

$$E_s = \frac{e_s \times N}{S}. \tag{3}$$

Here, e_s is the surface energy per atom in a nanoparticle and E_s is the surface energy of a nanoparticle (N is the total number of atoms in a nanoparticle and S is the surface area of a nanoparticle). We found that E_s decreases with decreasing temperature (Fig. 3). Moreover, we clearly found the size dependence of surface energy of nanoparticles; i.e., due to the surface effects, the smaller the nanoparticle, the higher the surface energy (Fig. 3).

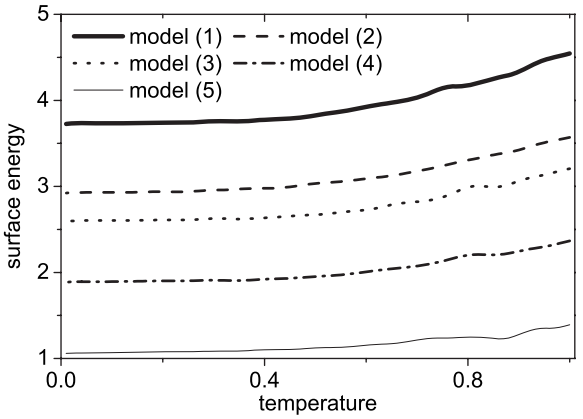

FIG. 3. Temperature dependence of the surface energy (E_s) of nanoparticles.

Like those noted above, the features of the glass transition in liquids are still unclear including glass transition in nanoscaled systems (i.e., nanoparticles, thin films, and liquids in confined geometries), which has been under intensive investigations in recent years.[8,30–32] While the glass transition temperature is typically lower in a confined geometry, experiments have also found cases where T_g increases.[33,34] The finite size effects on T_g cannot be readily interpreted as that on the melting temperature T_m due to the lack of a consensus on the nature of the glass transition.[35,36] The glass transition temperature in the present work was found via the intersection of a linear high- and low-temperature extrapolation of potential energy like those done for bulk Al_2O_3-SiO_2 (see Ref. 37 and Fig. 4). We found that T_g is equal to 0.386, 0.384, 0.392, 0.390, and 0.371 for models (1), (2), (3), (4), and (5), respectively. It is essential to note that the method of determining T_g in the present work is only an approximation; therefore, we suggest that T_g increases with decreasing nanoparticle size like that found experimentally for the glass tran-

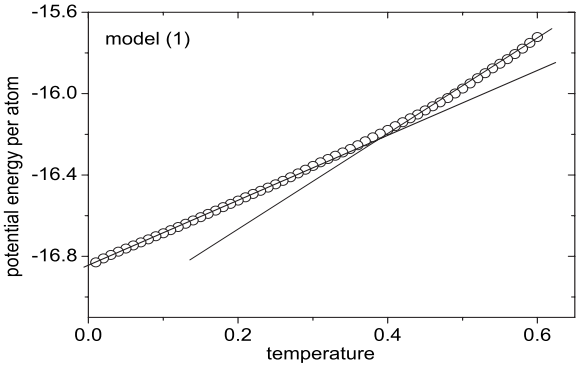

FIG. 4. Determination of T_g via an intersection of low- and high-temperature dependence of the potential energy of nanoparticles.

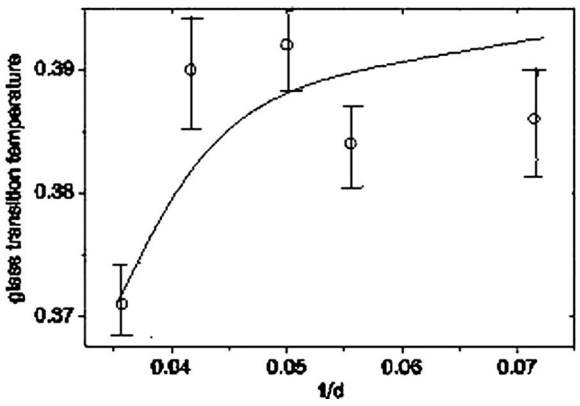

FIG. 5. An inverse nanoparticle size dependence of the glass transition temperature.

sition in liquid propylene glycol and two of its oligomers inside the pores of controlled porous glasses[34] (see Fig. 5; the solid line is just the suggested one for the inverse nanoparticle size dependence of T_g). The ideas behind most glass transition studies in the bulk were to probe the cooperative length involved in the glass transition, ξ. However, in confined systems at the nanoscale, they proposed new parameters which may influence the behavior of the glass transition. The first one is the size d of the nanoparticle and the atomic size σ may be considered as an additional parameter.[30] Moreover, the boundary conditions of confined geometries may affect the glass transition.[14] In the present work, we use a simple fixed and elastic reflection boundary, and our results give additional understanding of the glass transition in nanoscaled systems. In order to highlight some features of dynamics in the system upon cooling from the melt, the mean-squared displacement (MSD) of atoms in model (2) has been presented in Fig. 6. Like those commonly observed in glass-forming liquids, one can clearly see two regimes in the MSD curves: a ballistic one at short time and a diffusive one at longer time. At low temperatures, these two regimes are separated by a plateau regime. The plateau regime is related to the caging effects, which is more pronounced at lower temperatures. In addition, Fig. 6 also shows that at a temperature below the glass transition ($T=0.1$), atoms in the nanoparticle look mobile unlike that

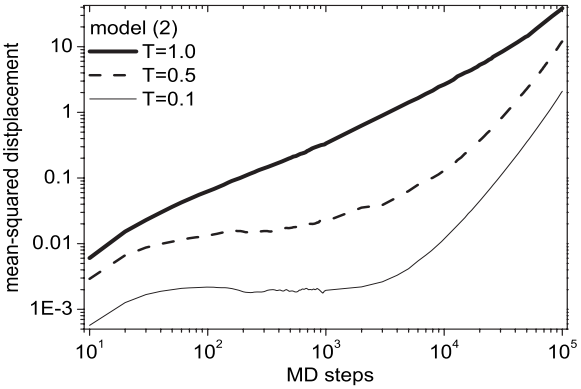

FIG. 6. MSD of atoms of nanoparticles at different temperatures.

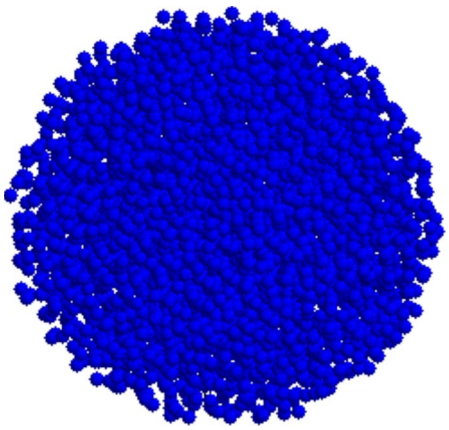

FIG. 7. (Color online) Snapshot of a well-relaxed amorphous nanoparticle with the size $d=20\sigma$ or model (3) obtained at $T=0.1$.

commonly observed in the bulk (i.e., after the ballistic regime, the MSD is almost constant for a long time due to strong caging effects), indicating the surface effects on the dynamics of atoms in the former.

B. Structural properties

The structural properties of amorphous nanoparticles are of great interest. Due to the surface effects, their structure may be different from the bulk counterparts. Moreover, while the structure of the latter was relatively well investigated, our understanding of the structure of the former is still limited, especially those of the monatomic amorphous nanoparticles.[12,13,15,38] Snapshot and static diffraction images of a well-relaxed amorphous nanoparticle with the size $d=20$ are presented in Figs. 7 and 8. We can clearly see the formation of a glassy state in the system, and the surface shell of an amorphous nanoparticle contains voids of different forms and sizes, which can be considered as structural point defects. Structural point defects in the surface shell can have an important role in the structure and physicochemical properties of nanosized substances.[4,13] We will return to this problem in subsequent parts of the paper.

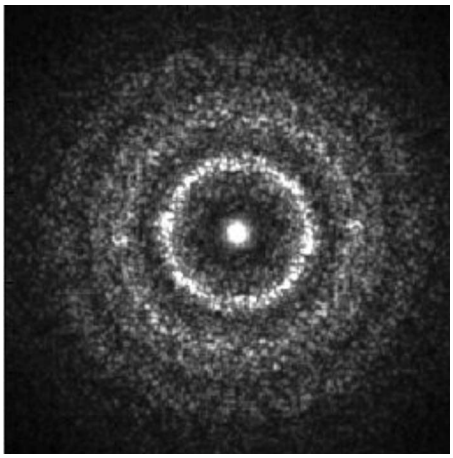

FIG. 8. Static diffraction image of a well-relaxed amorphous nanoparticle with the size $d=20\sigma$ or model (3) obtained at $T=0.1$.

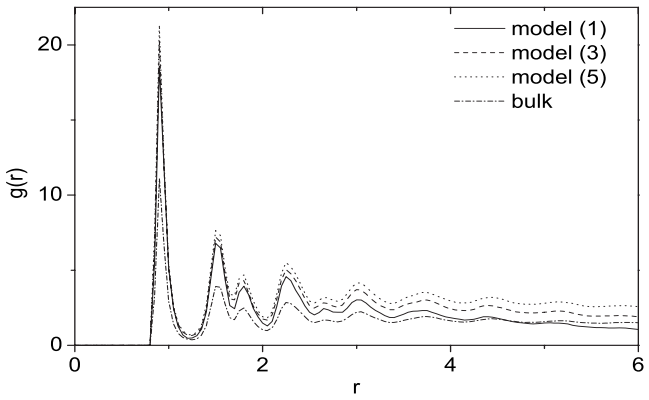

FIG. 9. RDF of well-relaxed amorphous nanoparticles obtained at $T=0.1$ compared with that observed in the bulk.

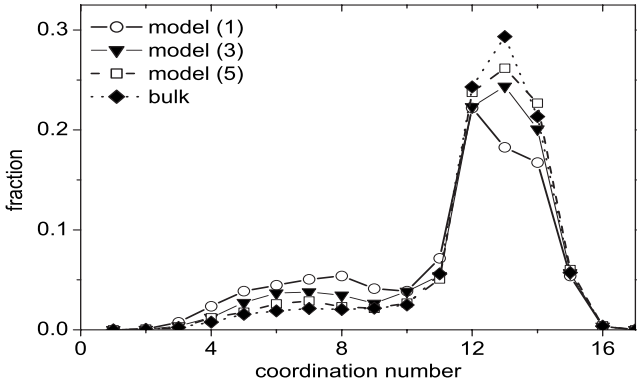

FIG. 10. Coordination number distributions of well-relaxed amorphous nanoparticles obtained at $T=0.1$ compared with that observed in the bulk.

In order to understand the atomic structure of liquids and glasses, the most widely used one is the RDF, and we found specific features of the RDF of amorphous nanoparticles in the present work (Fig. 9). First, we found that the RDF has a typical form that is very similar to that of metallic glasses, i.e., it has a first sharp peak with a split second peak.[39] The subpeak of the second peak in the RDF is often thought to be related to the existence of icosahedra in the system.[25,40,41] Indeed, we found the existence of the icosahedra in the system via the Honeycutt–Andersen local order analysis.[19] This means that one can use this simple monatomic LJG model for studying the nature of metallic glasses in addition to a similar Dzugutov model.[25,40] On the other hand, the peaks in the RDF of amorphous nanoparticles are broader than those of the bulk, indicating that the structure of the former is more heterogeneous than that of the latter due to the contribution of the surface structure. In addition, the RDF of amorphous nanoparticles is also size dependent, which can be clearly seen for the peaks beyond the second one, i.e., the larger the size of the nanoparticle, the higher the peaks in the RDF, which reflects the size dependence of the structure of amorphous nanoparticles in general (see Fig. 9). However, more detailed information about the size dependence of the structure of amorphous nanoparticles can be seen only via other structural properties.

We show the coordination number and bond-angle distributions for the entire nanoparticles in Figs. 10 and 11, and some remarks can be made. The coordination number distributions in amorphous nanoparticles and in the bulk counterpart are broad, indicating the disordered structure of the systems typical of metallic glasses. Many atoms in amorphous nanoparticles are located in the position surrounded by 12 nearest neighbors, which may be related to the icosahedra of 12 vertices in the system. In fact, we found the existence of 1551 bond pairs in the system, since the number of 1551 bonds is a direct measurement of the degree of icosahedral ordering in supercooled liquids and glasses.[19] One can see that the fraction of atoms with low coordination number decreases, while the fraction of atoms with high coordination number increases with increasing nanoparticle size toward that of the bulk, reflecting the surface effects [i.e., the ratio of the surface to volume S/V of nanoparticles decreases with increasing size (Fig. 10)]. In contrast, the mean interatomic distance in nanoparticles is size independent and equal to that of the bulk. Some characteristics of amorphous nanoparticles compared with those observed in the bulk can be found in Table II. On the other hand, the bond-angle distributions for amorphous nanoparticles have a single pronounced peak at 60°, indicating the dominance of equilateral triangles in the system, which may be related to the faces of icosahedra. We found that bond-angle distributions weakly depend on the nanoparticle size (Fig. 11).

One can discuss in more detail the spatial atomic configuration of amorphous nanoparticles by using the radial atomic density profile $\rho(R)$, where R is the distance from the center of the nanoparticle. This quantity is determined as follows: We find the number of atoms belonging to the spherical shell with the thickness of $\Delta R=0.2$ formed by two spheres with radii $R-0.1$ and $R+0.1$. Then we calculate the quantity $\rho(R)$, i.e., the number of atoms per unit volume at the distance R from the center of the nanoparticle. Here, it is unphysical if we begin with R from zero or from a very small value since the number of atoms in any volume element is small; the local density is a rather noisy variable. We show $\rho(R)$ only for three different nanoparticles; however, similar results have been found for nanoparticles with other sizes (Fig. 12). We can clearly see two parts of $\rho(R)$: The first one is related to the core of nanoparticle, whereas $\rho(R)$ is nearly constant up to $R\approx 4.2$, 6.5, and 9.3 for models (1), (3), and (5), respectively (see Fig. 12). The remaining part is related to the

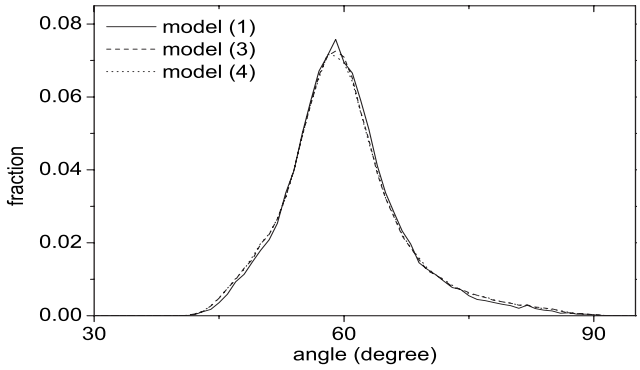

FIG. 11. Bond-angle distributions of well-relaxed amorphous nanoparticles obtained at $T=0.1$.

TABLE II. Several characteristics of amorphous nanoparticles compared with those observed in the bulk at the same $T=0.1$ (d and N are diameter and total number of atoms of the nanoparticle, T_g is a glass transition temperature, $\bar{r}$ is a mean interatomic distance, and $\bar{Z}$ is a mean coordination number; all quantities are given in LJ-reduced units). For the bulk, d means the length of a cube.

	Nanoparticles					
Quantity	Model (1)	Model (2)	Model (3)	Model (4)	Model (5)	Bulk
d	14	18	20	24	28	22.617
N	1189	2469	3407	5743	9093	9261
T_g	0.386	0.384	0.392	0.390	0.371	0.385
$\bar{r}$	0.904	0.904	0.904	0.904	0.904	0.904
$\bar{Z}$	11.149	11.539	11.745	11.947	12.107	12.237

surface of nanoparticles, whereas $\rho(R)$ is beginning to decrease down to zero. Figure 12 shows that $\rho(R)$ for the core of nanoparticles is nearly size independent, i.e., it has almost the same value for nanoparticles with three different sizes. This means that the core structure of simple amorphous nanoparticles may be similar to each other. The curve for $\rho(R)$ obtained in the present work is similar to those observed for KI nanoclusters[42] and it is unlike those found for amorphous TiO_2 nanoparticles[13] or silica nanoclusters.[43] For amorphous silica nanoclusters, it was found that oxygen has a tendency to concentrate at the surface and it causes a subsequent enrichment of Si atoms at the layer just below the surface in order to achieve the local charge neutrality. This phenomenon causes the occurrence of a peak in $\rho(R)$ anywhere close to the surface of nanoclusters, i.e., due to the chemical ordering in the system containing particles with different charges in addition to the different atomic sizes.[43] On the other hand, we can see in Fig. 12 that the real radii of nanoparticles are less than the "formal" radii, i.e., the real nanoparticle radii are around 6.1, 8.7, and 11.5 for models (1), (3), and (5), respectively. However, the radii for such models were taken equal to 7.0, 10.0, and 14.0, respectively (see Table II). The problem may be related to the relatively low density $\rho_0=0.8$ adopted for NVT ensemble simulation, and atoms have a tendency to aggregate with each other in order to achieve the most stable configuration (or the equilibrium configuration). According to our estimation, the "real" density (or the equilibrium density) of nanoparticles with the adopted LJG interatomic potential is approximately $\rho_0 \approx 1.20$. The same tendency was found for the bulk models, i.e., atoms also have a tendency to aggregate with each other in order to achieve the equilibrium density of a value higher than that adopted $\rho_0=0.8$ for the NVT ensemble simulation.

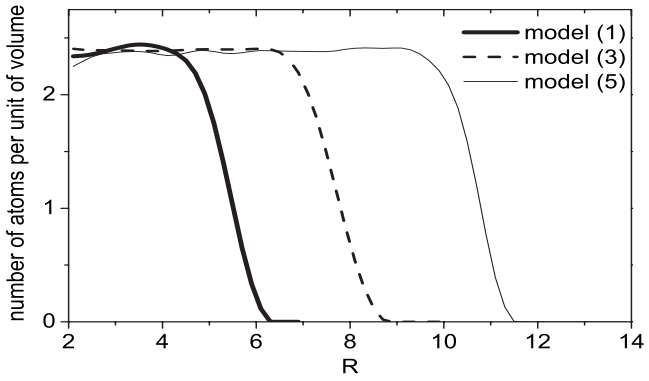

FIG. 12. Radial atomic density profile $\rho(R)$ of well-relaxed amorphous nanoparticles obtained at $T=0.1$.

Like those discussed above, the coordination number distributions in the core of amorphous nanoparticles are nearly size independent and are close to that of the bulk (Fig. 13). It is essential to note that the same phenomenon, i.e., the core structure of amorphous nanoparticles is nearly size independent, was found for amorphous SiO_2 or TiO_2 nanoparticles.[13,15] However, one can see that the atomic arrangements in the core of nanoparticles are more closely packed compared to that of the bulk, i.e., the fraction of atoms with high coordination number is higher, while the fraction of atoms with low coordination number is lower than that of the bulk. In contrast, the surface of amorphous nanoparticles has a more porous structure compared to that of the core or the bulk. The coordination number distributions in the surface shells are quite different from those of

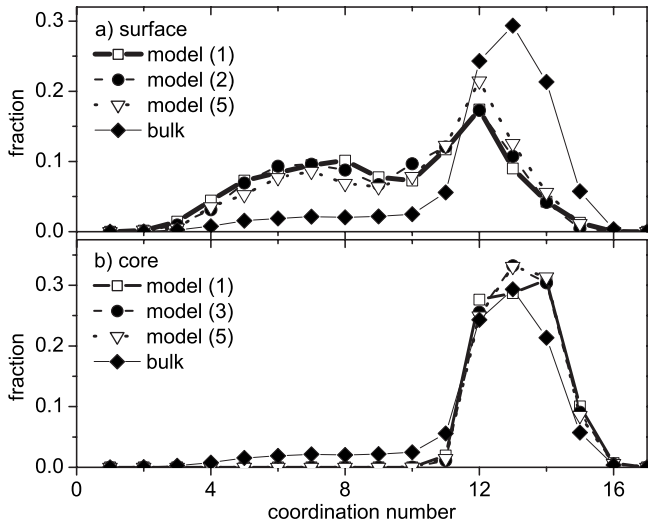

FIG. 13. Coordination number distributions (a) in the surface shells and (b) in the core of well-relaxed amorphous nanoparticles obtained at $T=0.1$.

TABLE III. Mean coordination number in the surface shell and in the core of amorphous nanoparticles at $T=0.1$.

	Model (1)	Model (3)	Model (5)
Surface	9.327	9.470	9.910
Core	13.215	13.223	13.223

the bulk or the core. We found that the coordination number distributions in the surface shells of amorphous nanoparticles are size dependent although weak (see Fig. 13 and Table III). One can see in Table III that the mean coordination number in the surface shell of amorphous nanoparticles is much less than that of the core. Since the mean coordination number for entire nanoparticles is around 11–12, undercoordinated structural units (for example, those with $Z \leqslant 6$) or overcoordinated ones (for example, those with $Z \geqslant 16$) compared to the mean one can be considered as the structural point defects. Our calculations show that such point defects mostly concentrate in the surface shells of amorphous nanoparticles rather than in the core.

One more type of structural defects in amorphous nanoparticles is vacancy, i.e., due to a specific disordered structure, there is a significant amount of large pores that can exchange position with the nearest neighbor atoms and they can act as vacancies in the diffusion processes like those found and discussed for amorphous Al_2O_3 (see Ref. 44). This means that the surface of amorphous nanoparticles contains a large amount of structural point defects such as vacancies and atoms with low coordination number (see Fig. 7), while the core has overcoordinated structural point defects if any. Due to the small dimension, probably, amorphous nanoparticles can have only such structural defects unlike those observed in crystalline nanosized substances.[4] The existence of structural defects at the surfaces of amorphous nanoparticles might enhance the diffusion of atomic species like those observed and discussed for silica nanoclusters.[43,45] Possibly, it is the origin of the different surface properties of amorphous nanoparticles, i.e., structural defects can play an important role in the structure and properties of amorphous nanoparticles including catalysis, adsorption, optical properties, etc., like those observed for nanocrystalline TiO_2 (see Ref. 4 and references therein). In fact, the strong red photoluminescence of amorphous SiO_2 nanoparticles has been attributed to the defects at their inner surfaces,[46] and it was pointed out that intrinsic point defects are the origin of optical band gap narrowing in fused silica nanoparticles.[47]

C. Evolution of structure upon cooling from the melts

In order to gain some insights into the transition from the liquid state to the glassy state, we present several structural characteristics of model (3) obtained upon cooling from the melt. We found that at relatively high temperature $T=1.0$, the second peak in the RDF of the system also has a small subpeak, which was thought to be related to the existence of icosahedron-type clusters in the system (Fig. 14). Figure 14 shows that (i) more pronounced changes have been observed

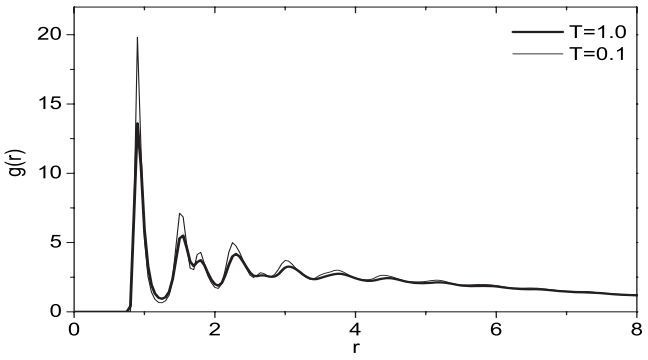

FIG. 14. RDF of unrelaxed amorphous nanoparticles with the size $d=20\sigma$ obtained at different temperatures upon cooling from the melt.

for the first peak in the RDF, that is, its magnitude is strongly enhanced and the width becomes narrower like those commonly found in glass-forming liquids;[48] (ii) the subpeak of the second peak is enhanced with decreasing temperature, indicating the increment of the fraction of icosahedra in the system; and (iii) the amplitude of oscillations are larger at lower temperature for peaks beyond the second ones. However, more details about the changes of structure upon cooling from the melt can be found via the coordination number distributions and atomic density profile (Figs. 15 and 16). The fraction of atoms with low coordination number decreases, while the fraction of atoms with high coordination number increases with decreasing temperature. This indicates the formation of a more close-packed structure in the system upon cooling from the melt due to the glass transition. Indeed, the mean coordination number increases from 11.112 to 11.753 when temperature decreases from $T=1.0$ to $T=0.1$ (Fig. 15). The evolution of another important quantity of the system caused by cooling from the melt, which is the atomic density profile $\rho(R)$, can be seen in Fig. 16. One can see that atoms have a tendency to concentrate in the core of nanoparticles and they move from the surface into the core when the system is cooling down; i.e., $\rho(R)$ decreases in the surface shell and it increases in the core of nanoparticles if temperature is lowered (Fig. 16).

In order to analyze the evolution of structure upon cooling from the melt in more detail, we use the common technique proposed by Honeycutt and Andersen.[19] The analysis was

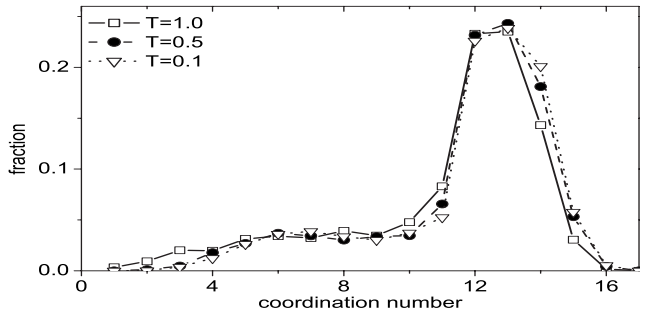

FIG. 15. Coordination number distributions of unrelaxed amorphous nanoparticles with the size $d=20\sigma$ obtained at different temperatures upon cooling from the melt.

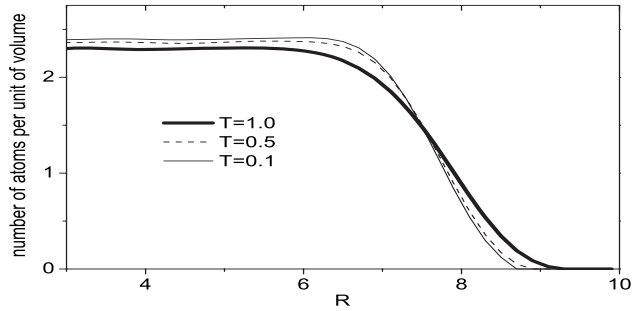

FIG. 16. Radial atomic density profile $\rho(R)$ of unrelaxed amorphous nanoparticles with the size $d=20\sigma$ obtained at different temperatures upon cooling from the melt.

done by using a special program written by Hoang. The structure is analyzed by pairs of atoms, which are classified via four indices: (i) The first index indicates whether or not they are near neighbors. The first index is 1 if the pair is bonded and 2 otherwise, and we use the fixed cutoff radius $R_o=1.25$ for determining the nearest-neighbor behavior. (ii) The second index is equal to the number of near neighbors they have in common. (iii) The third index is equal to the number of bonds among common near neighbors. (iv) The fourth index is related to the arrangement of the bonds among the common near neighbors (Fig. 17). Indeed, we found the existence of various pairs of bonds like those obtained for Lennard-Jones liquids[19] (see Table IV). However, the most abundant pairs are just 2101, 2211, 2331, 2441, 1551, 1541, and 1661, and their temperature dependence can be seen in Fig. 18. One can see that the fraction of the 1551 pair increases with decreasing temperature, indicating the enhancement of icosahedral local order in the system like those stated via the changes in the intensity of the subpeak of the second peak in RDF. However, the existence of other pairs such as 2101, 2211, and 2331 in large amount shows the existence of other local orders in the system. It is essential to note that local icosahedral symmetry was also found in con-

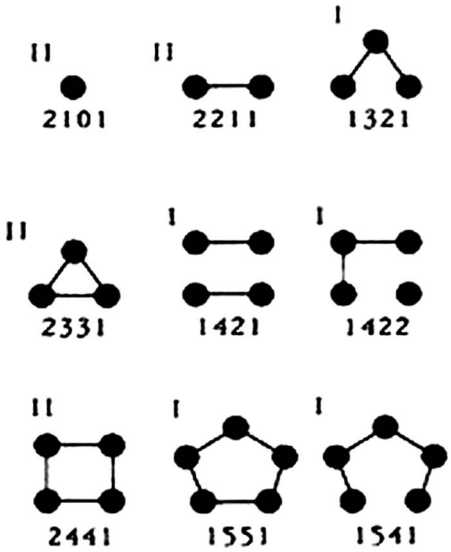

FIG. 17. Common pair bond diagrams in supercooled liquids (Ref. 19).

TABLE IV. The abundance (fraction) of various bond pairs in unrelaxed model (3).

Pair	$T=1.0$	$T=0.6$	$T=0.2$
2101	0.391	0.373	0.364
2211	0.182	0.170	0.169
2331	0.231	0.255	0.260
2441	0.018	0.017	0.020
1301	0.002	0.001	0.001
1311	0.011	0.008	0.007
1321	0.010	0.010	0.009
1421	0.004	0.003	0.002
1422	0.011	0.007	0.006
1441	0.004	0.005	0.006
1551	0.089	0.104	0.108
1541	0.035	0.033	0.031
1661	0.011	0.013	0.016

fined amorphous LJ argon,[17] in LJ clusters,[24] or in several metallic nanoclusters such as silver,[49] gold,[50–52] copper,[53,54] nickel,[55] and lead.[56] In particular, the freezing of Lennard-Jones clusters[24] with $160<N<2200$ was studied by MD simulations (N is the total number of atoms in clusters) and they found that there was a transition at increasing size from icosahedra to a mixture of structures (decahedron, fcc, hcp, and icosahedron). The transition did not depend on the cooling method and took place for $N\cong 450$ (see Ref. 24). Our calculations for the LJG nanoparticles indicate that they have a mixture of structures for the whole temperature range studied since there are different bond pairs in large amount in addition to the 1551 bond pair and the fraction of different bond pairs does not change much with increasing size of nanoparticles from that containing 1189 atoms to that containing 9093 atoms.

D. Aging effects

Aging effects on the structure and properties of glasses were given much attention in recent years by both experi-

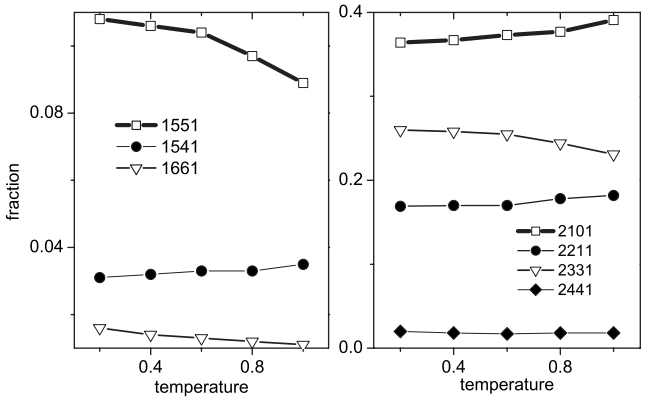

FIG. 18. Temperature dependence of bond pairs of unrelaxed amorphous nanoparticles with the size $d=20\sigma$.

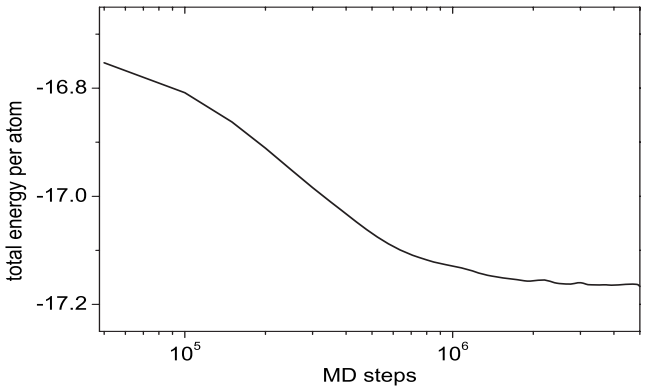

FIG. 19. Aging time dependence of total energy per atom in an amorphous nanoparticle with the size $d=18\sigma$ at constant $T=0.3$.

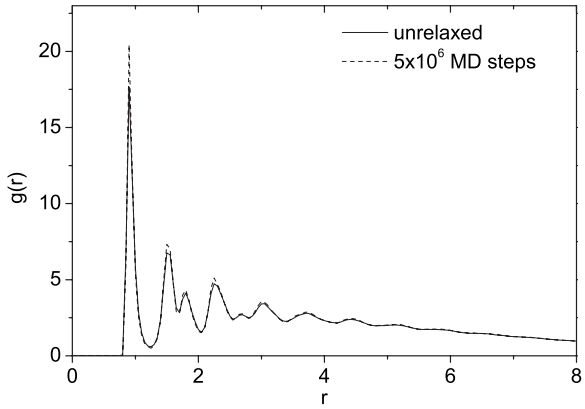

FIG. 20. RDF of an amorphous nanoparticle with the size $d=18\sigma$ obtained after different aging times at constant $T=0.3$.

ments and computer simulations.[57–65] However, due to the limitation of computer power, the aging problem in glasses is a serious challenge for the computer simulation community. Therefore, there is a limited number of works related to the study of aging in glasses by using computer simulations and much attention was paid just for the bulk glasses.[57,59–65] To the best of our knowledge, there is no MD simulation work related to the investigation of aging effects in amorphous nanoparticles. It motivates us to carry out the study in this direction, and model (2) obtained by cooling from the melt at $T=0.3$ was relaxed at constant temperature and constant volume (i.e., *NVT* ensemble simulation) up to 5×10^6 MD steps (or 6.175 ns if Ar is taken for testing) in order to investigate the aging effects. Like those observed for the bulk Al_2O_3 (see Refs. 63–65), the aging time dependence of the total energy of the amorphous nanoparticle in the present work also has two different parts (Fig. 19): The first one is related to the early time window of $0\leqslant n\leqslant10^6$ (n denotes the number of MD steps; the model with $n=0$ is related to the unrelaxed one), the second one is related to the later time window of $10^6<n\leqslant5\times10^6$. The total energy in the first part of the curve is high and rapidly decreases with the aging time, indicating that the initial model, which was obtained by cooling from the melt, is far from the equilibrium state. In contrast, the total energy in the second part of the curve is nearly constant with the aging time, indicating the achievement of an equilibrium state of the system after aging long enough.

It was found that the static properties of glasses do not significantly depend on aging.[57,59,63–65] Almost the same situation was found for the aging effects on the static properties of the amorphous nanoparticles. We found that aging just slightly changes the RDF and the atomic density profile of amorphous nanoparticles (Figs. 20 and 21). However, some remarks can be made here. Aging leads to a slight increase in the height of peaks in the RDF, especially for the first peak, indicating the enhancement of structural order in the nanoparticles. Indeed, we found that the mean coordination number slightly increases from 11.516 to 11.677 after aging an unrelaxed model for 5×10^6 MD steps. The same tendency was found for the bulk supercooled Al_2O_3. On one hand, aging also leads to a slight movement of atoms from the surface into the core of the amorphous nanoparticle, i.e., atomic density decreases in the surface shell, while it increases in the core of the nanoparticle (see Fig. 21). On the other hand, since an amorphous structure of LJG nanoparticles remains unchanged during the relatively long aging of 6.175 ns, one can suggest that amorphous LJG nanoparticles are practically stable in the sense that no crystallization occurs during relatively long annealing like that found for the bulk counterpart. Moreover, it was found that confinement can greatly enhance the stability of amorphous structure of nanoscaled systems compared to that observed in the bulk.[17]

IV. CONCLUSIONS

Simple monatomic amorphous nanoparticles with the LJG interatomic potential have been obtained by using MD method. Calculations show that a practically stable glassy state can be obtained by using the LJG potential. We found the size effects on static properties and on thermodynamic quantities of amorphous nanoparticles. It was found that the glass transition temperature of LJG nanoparticles has a tendency to increase with decreasing nanoparticle size like that found experimentally for liquid propylene glycol and two of its oligomers inside the pores of controlled porous glasses.[34]

Amorphous nanoparticles have two distinct parts: the surface and the core. The structure of the former is size depen-

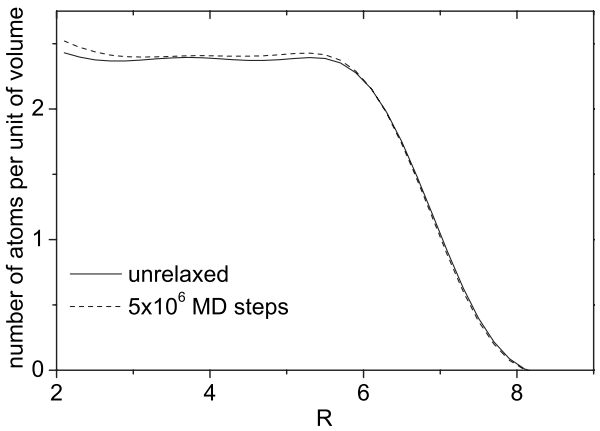

FIG. 21. Radial atomic density profiles of an amorphous nanoparticle with the size $d=18\sigma$ obtained after different aging times at constant $T=0.3$.

dent, with typically low atomic density. The surface of amorphous nanoparticles contains a large amount of structural defects, which may have an important role in the structure and properties of nanoparticles. In contrast, the core of amorphous nanoparticles has a more close-packed structure compared to that of the surface and nearly size independent.

We found the existence of icosahedral local order in the glassy state with LJG interatomic potential like those often observed in metallic glasses or in those of Dzugutov. We found that the icosahedral local order in the system is enhanced upon cooling from the melt. Moreover, upon cooling from the melt, atoms have a tendency to move from the surface into the core of amorphous nanoparticles.

Like those previously observed in glasses, the static properties of amorphous nanopaticles do not depend significantly on aging. However, we found that aging leads to the slight enhancement of local structural order and also leads to a slight movement of atoms from the surface into the core of amorphous nanoparticles.

Since there are only a few works related to the amorphous nanoparticles, our results give additional understanding of the important forms of the different polymorphs of nanoparticles.

ACKNOWLEDGMENTS

One of the authors (V.V.H.) thanks the financial support from the Japan Society for Science Promotion. The authors thank D. K. Belashchenko for providing the MD program. This work was supported in part by the Grant-in-Aid for Scientific Research from the Ministry of Education, Culture, Sports, Science and Technology of Japan.

*vvhoang2002@yahoo.com

[1] M. L. Steigerwald, A. P. Alivisatos, and L. E. Brus, Annu. Rev. Mater. Sci. **19**, 471 (1989).
[2] M. L. Cohen and W. D. Knight, Phys. Today **43**(12), 42 (1990).
[3] R. W. Siegel, Phys. Today **46**(10), 64 (1993).
[4] U. Diebold, Surf. Sci. Rep. **48**, 53 (2003).
[5] X. Chen and S. S. Mao, Chem. Rev. (Washington, D.C.) **107**, 2891 (2007).
[6] Yi Yang, V. J. Leppert, S. H. Risbud, B. Twanley, P. P. Power, and H. W. H. Lee, Appl. Phys. Lett. **74**, 2262 (1999).
[7] H. Yasuda, K. Mitsuishi, and H. Mori, Phys. Rev. B **64**, 094101 (2001).
[8] Z. Zhang, M. Zhao, and Q. Jiang, Physica B **293**, 232 (2001).
[9] J. G. Lee, H. Mori, and H. Yasuda, Phys. Rev. B **66**, 012105 (2002).
[10] G. Kataby, Yu. Koltypin, A. Ulman, I. Felner, and A. Gedanken, Appl. Surf. Sci. **201**, 191 (2002).
[11] L. Machala, Z. Zboril, and A. Gedanken, J. Phys. Chem. B **111**, 4003 (2007).
[12] A. Galashev, V. Polukhin, I. Izmodenov, and O. Rakhmanova, Glass Phys. Chem. **32**, 99 (2006).
[13] V. V. Hoang, H. Zung, and N. H. B. Trong, Eur. Phys. J. D **44**, 515 (2007).
[14] J. D. McCoy and J. G. Curro, J. Chem. Phys. **116**, 9154 (2002).
[15] V. V. Hoang, J. Phys. Chem. B **111**, 12649 (2007).
[16] F. Baletto and R. Ferrando, Rev. Mod. Phys. **77**, 371 (2005).
[17] K. Nishio, J. Koga, T. Yamaguchi, and F. Yonezawa, J. Phys. Soc. Jpn. **73**, 627 (2004).
[18] C. L. Briant and J. J. Burton, J. Chem. Phys. **63**, 2045 (1975).
[19] J. D. Honeycutt and H. C. Andersen, J. Phys. Chem. **91**, 4950 (1987).
[20] D. D. Frantz, J. Chem. Phys. **102**, 3747 (1995).
[21] A. Rytkonen, S. Valkealahti, and M. Manninen, J. Chem. Phys. **106**, 1888 (1997).
[22] A. Rytkonen, S. Valkealahti, and M. Manninen, J. Chem. Phys. **108**, 5826 (1998).
[23] D. D. Frantz, J. Chem. Phys. **115**, 6136 (2001).
[24] T. Ikeshoji, G. Torchet, M.-F. de Feraudy, and K. Koga, Phys. Rev. E **63**, 031101 (2001).
[25] M. Dzugutov, Phys. Rev. A **46**, R2984 (1992).
[26] M. Engel and H.-R. Trebin, Phys. Rev. Lett. **98**, 225505 (2007).
[27] C. H. Cho, S. Singh, and G. W. Robinson, Faraday Discuss. **103**, 19 (1996).
[28] P. A. Netz, J. F. Raymundi, A. S. Camera, and M. C. Barbosa, Physica A **342**, 48 (2004).
[29] M. C. Rechtsman, F. H. Stillinger, and S. Torquato, Phys. Rev. E **74**, 021404 (2006).
[30] Y. Xia, G. Dosseh, D. Morineau, and C. Alba-Simionesco, J. Phys. Chem. B **110**, 19735 (2006).
[31] C. L. Jackson and G. B. McKenna, J. Non-Cryst. Solids **131-133**, 221 (1991).
[32] J. Zhang, G. Liu, and J. Jonas, J. Phys. Chem. **96**, 3478 (1992).
[33] X. Wang and W. Zhou, Macromolecules **35**, 6747 (2002).
[34] J. Schuller, Y. B. Melnichenko, R. Richert, and E. W. Fischer, Phys. Rev. Lett. **73**, 2224 (1994).
[35] C. L. Jackson and G. B. McKenna, Chem. Mater. **8**, 2128 (1996).
[36] Q. Jiang, H. S. Shi, and M. Zhao, J. Chem. Phys. **111**, 2176 (1999).
[37] V. V. Hoang, Phys. Rev. B **75**, 174202 (2007).
[38] N. N. Linh and V. V. Hoang, NANO **2**, 227 (2007).
[39] D. K. Belashchenko, *Structure of Liquid and Amorphous Metals* (Metalurgia, Moscow, 1985) (in Russian).
[40] M. Dzugutov, J. Non-Cryst. Solids **156-158**, 173 (1993).
[41] Li Hui, D. Feng, B. Xiufang, and W. Guanghou, Chem. Phys. Lett. **354**, 466 (2002).
[42] J. Huang and L. S. Bartell, J. Mol. Struct. **567-568**, 145 (2001).
[43] A. Roder, W. Kob, and K. Binder, J. Chem. Phys. **114**, 7602 (2001).
[44] V. V. Hoang, Phys. Rev. B **70**, 134204 (2004).
[45] I. V. Schweigert, K. E. J. Lehtinen, M. J. Carrier, and M. R. Zachariah, Phys. Rev. B **65**, 235410 (2002).
[46] A. Colder, F. Huisken, E. Trave, G. Ledoux, O. Guillois, C. Reynaud, H. Hofmeister, and E. Pippel, Nanotechnology **15**, L1 (2004).
[47] A. Stesmans, K. Clemer, and V. V. Afanas'es, J. Phys.: Condens. Matter **17**, L393 (2005).
[48] K. Vollmayr, W. Kob, and K. Binder, Phys. Rev. B **54**, 15808

(1996).
[49] F. Baletto, C. Mottet, and R. Ferrando, Chem. Phys. Lett. **354**, 82 (2002).
[50] Y. G. Chushak and L. S. Bartell, Eur. Phys. J. D **16**, 43 (2001).
[51] Y. G. Chushak and L. S. Bartell, J. Phys. Chem. B **105**, 11605 (2001).
[52] H.-S. Nam, N. M. Hwang, B. D. Yu, and J.-K. Yoon, Phys. Rev. Lett. **89**, 275502 (2002).
[53] S. Valkealahti and M. Manninen, J. Phys.: Condens. Matter **9**, 4041 (1997).
[54] D. Reinhard, B. D. Hall, P. Berthoud, S. Valkealahti, and R. Monot, Phys. Rev. Lett. **79**, 1459 (1997).
[55] Y. Qi, T. Cagin, W. L. Johnson, and W. A. Goddard III, J. Chem. Phys. **115**, 385 (2001).
[56] H. S. Lim, C. K. Ong, and F. Ercolessi, Comput. Mater. Sci. **2**, 495 (1994).
[57] H. Miyagawa and Y. Hiwatari, Phys. Rev. A **40**, 6007 (1989).
[58] H. Hirashima, M. Gengyo, C. Kojima, and H. Imai, J. Non-Cryst. Solids **186**, 54 (1995).
[59] W. Kob and J.-L. Barrat, Phys. Rev. Lett. **78**, 4581 (1997).
[60] B. Doliwa and A. Heuer, J. Non-Cryst. Solids **307-310**, 32 (2002).
[61] A. Kerrache, V. Teboul, D. Guichaoua, and A. Monteil, J. Non-Cryst. Solids **322**, 41 (2003).
[62] N. Giovambattista, H. E. Stanley, and F. Sciortino, Phys. Rev. E **69**, 050201(R) (2004).
[63] V. V. Hoang and S. K. Oh, Phys. Rev. E **70**, 061203 (2004).
[64] V. V. Hoang and S. K. Oh, Physica B **364**, 225 (2005).
[65] V. V. Hoang, Physica B **367**, 210 (2005).